Pressure-loss coefficient of 90° sharp-angled mitre elbows

Wameedh T.M. Al-Tameemi
Ph.D. student, Department of Mechanical Engineering, University of Sheffield, Sheffield, UK
Reconstruction and Projects Office, Ministry of Higher Education and Scientific Research, Baghdad, Iraq
Email: wtal-tameemi1@sheffield.ac.uk

Pierre Ricco
Senior Lecturer in Fluid Mechanics, Department of Mechanical Engineering, University of Sheffield, Sheffield, UK
Email: p.ricco@sheffield.ac.uk

ABSTRACT

Accepted for publication in ASME Journal of Fluids Engineering

The pressure drop across 90° sharp-angled mitre elbows connecting straight circular pipes is studied in a bespoke experimental facility by using water and air as working fluids flowing in the range of bulk Reynolds number $500<\mathcal{R}e<60000$. *To the best of our knowledge, the dependence on the Reynolds number of the pressure drop across the mitre elbow scaled by the dynamic pressure, i.e. the pressure-loss coefficient* $\mathcal{K}$*, is reported herein for the first time. The coefficient is shown to decrease sharply with the Reynolds number up to about* $\mathcal{R}e=20000$ *and, at higher Reynolds numbers, to approach mildly a constant* $\mathcal{K}=0.9$*, which is about 20% lower than the currently reported value in the literature. We quantify this relation and the dependence between* $\mathcal{K}$ *and the straight-pipe friction factor at the same Reynolds number through two new empirical correlations, which will be useful for the design of piping systems fitted with these sharp elbows. The pressure drop is also expressed in terms of the scaled equivalent length, i.e. the length of a straight pipe that would produce the same pressure drop as the elbow at the same Reynolds number.*

Keywords: Pressure-loss coefficient, 90° sharp-angled elbow, turbulent flow, mitre elbows, pipe flow, pressure drop.

1 Introduction

Pipe fittings like elbows, bends and valves are essential in many industrial applications, such as hydraulic, nuclear and chemical engineering systems, and the prediction of the pressure drop across these fittings is crucial in the design of piping systems. Estimating these losses is more difficult than in straight pipe flows due to the additional sources of local energy dissipation caused by secondary flow and flow separation [1]. For round elbows, the pressure drop is inversely proportional to the curvature ratio $C=R^*/D^*$, where R^* is the elbow curvature radius and D^* is the diameter of the elbow [2]. (The symbol $*$ henceforth indicates a dimensional quantity, while quantities with no symbols are dimensionless.) Sharp-angled elbows suffer from higher localized losses than round elbows due to the even more intense flow separation [3, 4].

Several studies in the literature have investigated the pressure loss in 90° round elbows and bends in laminar flows [5, 6, 7] and turbulent flows [8, 9], while only three papers have presented results on the pressure loss in 90° sharp-angled mitre elbows [10, 11, 12]. Kirchbach [10] and Schubart [11] investigated the pipe-flow pressure drop of water flowing through smooth and rough 90° mitre elbows, respectively. The pressure-loss coefficient $\mathcal{K}$, i.e. the pressure drop across the elbow scaled by the dynamic pressure, was found to be approximately equal to 1.1. Haidar [12] measured the mitre-elbow pressure-loss coefficient for compressible air flows to be in the range $1.3-1.6$. Moujaes and Aekula [13] found that the pressure loss coefficient in 90° mitre ducts with rectangular cross section varies between 1.22 and 1.3 at a bulk Reynolds number of more than 10^5 by using numerical calculations. Books on fluid mechanics, for example Munson[14], White [15], and Rennels and Hudson [16], and engineering manuals, for example Crane [17], rely on Kirchbach's [10] and Schubart's [11] data and do not report any dependence of the pressure-loss coefficient of 90° mitre elbows on the bulk Reynolds number. Crane [17] used the experimental data of Kirchbach [10] to correlate these pressure-loss coefficients with the friction factor in straight pipes at the same Reynolds number.

The method of the equivalent length, developed by Ito [9], has also been used extensively to express the pressure drop across elbows and junctions [18, 4]. The equivalent length is the length of a straight pipe that would produce the same pressure drop as the elbow at the same Reynolds number. For 90° round elbows, the equivalent length for turbulent flows, when scaled with the diameter, has been shown to vary between 20 and 60 depending on the curvature ratio C [19, 18, 20]. Crawford [4] used a T shape junction with one blocked side to measure the equivalent length in 90° sharp-angled elbows and found it to be approximately equal to 45. An empirical formula for estimating the equivalent length for 90° elbows as a function of C at high flow rates was also proposed [3, 4].

It is evident that there is a dearth of studies relating minor pressure-loss coefficients for pipe fittings, especially 90° sharp-angled mitre elbows, with the Reynolds number. A symptomatic sentence on this point is found in White [15]: "Although $\mathcal{K}$ is dimensionless, it is often not correlated in the literature with the Reynolds number...". Motivated by this, we have carried out an experimental investigation of the pipe flow through 90° sharp-angled circular mitre elbows by varying the bulk Reynolds number $\mathcal{R}e=\mathcal{U}_b^* D^*/\nu^*$ (where $\mathcal{U}_b^*$ is the mean velocity and D^* is the pipe diameter) between 500 and 60000. We have utilized both air and water as working fluids in the same experimental facility and we have employed three diameters for each fluid. Other objectives of the study are to relate the pressure-drop coefficient of the elbow with the straight-pipe friction factor, to obtain empirical correlations for the pressure-drop coefficient, and to quantify the pressure drop in terms of the equivalent length.

2 Experimental apparatus and procedure

A new experimental apparatus was designed and built for this work in the Department of Mechanical Engineering at The University of Sheffield. The apparatus consisted of two main lines, one for air and one for water. They both fed the test section, where the sharp-angled elbows were located. The experimental facility is shown schematically in Fig. 1.

2.1 Air and water lines

Water was pumped from a 150 litres capacity water storage tank to the test section by a variable speed pump operating at constant pressure and a maximum flow rate of 80 l/min (litres per minute). The pump control unit consisted of a variable speed controller, a pressure transducer, a pressure gauge, a manual flow control valve and a potentiometer. This unit had the function of controlling the pump velocity to obtain a constant pressure at the exit of the pump for all the flow rates. The potentiometer and the pressure gauge were employed to set the pressure to the operating value. In case of any change in the flow pressure at different flow rates the pressure transducer sent a signal to the variable speed

controller to change the pump speed automatically and to keep the pressure constant at the new flow rate.

Two water filters were located before the pump to minimize the intrusion of impurities in the test sections. The water flow rates were measured by two different turbine types flow meters, Omega FTB-101 and Omega FTB-104, to cover two wide ranges of volume flow rates: 1.3-13.2 l/min and 6.6-60 l/min, respectively. The flow meters were calibrated by the manufacturer with a $\pm 0.5\%$ reading accuracy. A six digits rate meter (Omega DPF-702) was utilized to display the flow meters readings in l/min and manual separation valves were employed to close the water line when operating the rig with air.

Air was supplied by an air compressor and regulated to the required flow rate by a pressure valve. An air filter-dryer was located before the air flow meter to supply the test section with clean dry air. An air mass flow meter (FMA-1612A-v2) was used to measure the flow rates between 2.5 and 500 standard l/min. The flow meter was calibrated by the manufacturer with an accuracy of $\pm 0.8\%$ of the reading value and $\pm 0.2\%$ of the full scale value (FS).

2.2 Test sections

The test sections were constructed from commercial acrylic pipes with a wall thickness of 2mm, three different diameters (D^*=11, 16, and 21mm), and a total length of $240D^*$ for all the diameters ($100D^*$ upstream of the elbow and $140D^*$ downstream of the elbow to ensure full recovery of the flow). An additional straight $100D^*$-long pipe was located upstream of the test sections to ensure fully developed flow condition.

The test sections were assembled from segments which were joined together by using acrylic flanges. The flanges were designed carefully to seal the junctions between the pipe segments by using O-rings in order not to perturb the flow. The 90° sharp-angled elbows for all of the test sections were constructed by cutting two pipe pieces at 45°, which were joined accurately by using a special acrylic glue, as shown in Fig. 2.

Ten measurement stations were located along each test section to measure the pressure distribution along the straight parts of the pipe and across the elbow, as shown in Fig. 3. The pressure taps were designed and machined from the same material of the test sections. Holes with a diameter of 1mm were bored radially through the pipe walls to allow the fluid to flow through the pressure taps without perturbing the flow inside the pipe. M5 push-in fittings with 6mm flexible tubes were used to connect the pressure taps with the pressure measurement instruments. Two other pressure taps were located at four measurement stations upstream and downstream of the elbow in order to conduct peripheral pressure measurements at different angles around the pipe diameter (0° at the top, 90°, and 270°), as shown in Fig. 4.

2.3 Data acquisition and procedure

Two differential pressure transducers, Omega PX409-2.5DWU10V and Omega PX409-10WDWUI, were used to measure the water-flow pressure drop along the test sections. The transducers were calibrated by the manufacturer with an FS best straight line (BSL) accuracy of $\pm 0.08\%$. A differential water manometer, used to measure the air flow pressure drop, operated in a range of $0-4.9$kPa with $\pm 0.1\%$ of the reading value and ± 1Pa accuracy at $20^\circ C$. An absolute pressure transducer (PX309-100G5V) was employed to measure the absolute pressure in a range of $0-680$kPa and it was calibrated by the manufacturer with a $\pm 0.25\%$ FS BSL uncertainty. A National Instrument data acquisition system with 16-bit resolution and a special Labview code were used for the logging and processing of the pressure measurements. A type K thermocouple was used with a Picco data logger to measure the flow temperature at each experimental run. The thermocouple was carefully calibrated against an accurate thermometer

with less than $\pm$ 0.5°C accuracy.

The pressure along the test sections was measured at different flow conditions as listed in Table 1. The methodologies to compute the pressure-loss coefficient due to the elbow and the equivalent length to diameter ratio are presented in Appendix A. All of the experiments were conducted at about 25°C. The maximum change of the fluid temperature in all the experiments was about 5°C. Several experiments were repeated at different dates to check the repeatability of the measurements. The maximum deviation of the measured data across all the repeated experiments was about 0.7%. The pressure was shown to be axially symmetric along the pipe diameter at all the tested locations, as discussed in Appendix B.

2.4 Uncertainty analysis

There were two main sources of uncertainty: the uncertainty associated with the measurement instruments and the uncertainty in the measured values. The uncertainties of the measurement instruments were provided by the manufacturers, as discussed in Section 2.3. The uncertainties in the measured values included the uncertainty of the pipe diameter, the distance between the measurement stations, the roughness of the pipes, the elbow angles and the fluids properties. Each pipe diameter was measured carefully by a micrometer at five different locations with a $\pm$0.1mm maximum error, while the internal surface roughness of the pipe was measured by a Dektal 150 surface profiler with a $\pm$2% uncertainty. The distance between measurement stations was measured with a $\pm$1mm maximum error and the angle of the elbows was measured by an accurate protractor with a $\pm$0.5° uncertainty. The uncertainty in the fluid properties was computed for each experiment by using the NIST Refprop database [21]. The square root of the sum of the sequence method was used to obtain the total uncertainty of a measured quantity $f = f(x_0, .., x_N)$, as follows [22]:

$$\delta f = \sqrt{\sum_{n=0}^{N} \left(\frac{\partial f}{\partial x_n} \, \delta x_n \right)^2}, \tag{1}$$

where δx_n is the experimental error associated with the variable x_n. The uncertainties are indicated by error bars in the graphs of Section 3. For clarity, error bars are only shown for data corresponding to three or four representative Reynolds numbers rather than displaying the error bars for all data points.

3 Results

Before studying the local pressure drop due to the elbow, it is essential to verify that the Darcy friction factor of the turbulent flow in the straight pipe upstream of the elbow,

$$\mathcal{C}_f = \frac{2D^* \Delta p^*}{l^* \rho^* \mathcal{U}_b^{*2}}, \tag{2}$$

agrees with well-established empirical correlations for the range of Reynolds numbers of interest in our study. In Eq. (2) Δp^* is the pressure drop along the straight section of the pipe upstream of the elbow, l^* is the distance along which Δp^* is measured, ρ^* is the density of the fluid, $\mathcal{U}_b^* = \dot{m}^* / (\rho^* \mathcal{A}^*)$ is the mean-flow velocity, $\dot{m}^*$ is the mass flow rate, and $\mathcal{A}^*$ is the cross-sectional area of the pipe. Figure 5 shows $\mathcal{C}_f$ as a function of the Reynolds number $\mathcal{R}e = \mathcal{U}_b^* D^* / \nu^*$, where ν^* is the kinematic viscosity of the fluid, for the three different pipe diameters and the two fluids. The data are compared with Churchill's [23], Haaland's [24] and McKeon's [25] correlations and with data from experiments and direct numerical simulations [26, 27, 25, 28]. A very good agreement with less than $\pm$5% average error

is found. The scatter is almost constant in the whole Reynolds number range, although the estimated uncertainty increases as $\mathcal{R}e$ decreases. Air and water data have the same average errors.

The local pressure drop due to the 90° sharp-angled elbow is quantified by the pressure-loss coefficient $\mathcal{K}$, defined as:

$$\mathcal{K} = \frac{2\Delta p_e^*}{\rho^* \mathcal{U}_b^{*2}}, \tag{3}$$

where Δp_e^* is the pressure drop due to the elbow. Figure 6 shows $\mathcal{K}$ as a function of $\mathcal{R}e$. To the best of our knowledge, this is the first time that the dependence of $\mathcal{K}$ on $\mathcal{R}e$ has been presented for 90° sharp-angled mitre elbows. The experimental results show that $\mathcal{K}$ decreases rapidly as $\mathcal{R}e$ increases up to $\mathcal{R}e \approx 10^4$. For $\mathcal{R}e > 10^4$ the effect of $\mathcal{R}e$ is moderate as $\mathcal{K}$ keeps decreasing. As remarked by Munson [14] it is expected that the coefficient $\mathcal{K}$ displays a weak dependence on $\mathcal{R}e$ at high $\mathcal{R}e$ because the dominance of inertia effects, which is responsible for secondary flows and separation, renders the local pressure drop directly proportional to the dynamic pressure $0.5\rho^* \mathcal{U}_b^{*2}$. A new correlation based on our experimental data is proposed:

$$\mathcal{K} = 427.5\mathcal{R}e^{-0.77} + 0.9, \quad 500 \leq \mathcal{R}e \leq 60000. \tag{4}$$

Correlation (4) fits our experimental data within an average error of ±3%. The experimental data for smooth elbows by Kirchbach [10] and for rough elbows by Schubart [11] are shown for comparison in Fig. 6. Probably due to the high uncertainty in their experiments, Kirchbach's [10] and Schubart's [11] data do not show the subtle dependence of $\mathcal{K}$ on $\mathcal{R}e$ in the range $15000 < \mathcal{R}e < 60000$. They predict a constant $\mathcal{K}=1.1$, whereas our $\mathcal{K}$ values decrease slowly with $\mathcal{R}e$ and are consistently lower than theirs in this $\mathcal{R}e$ range. According to Kirchbach's [10] and Schubart's [11] data, roughness has no effect on $\mathcal{K}$ in this $\mathcal{R}e$ range, arguably because the Reynolds number is large enough for the elbow pressure drop to be caused mainly by the local separation rather than by frictional effects. As for the $\mathcal{C}_f$ data, our $\mathcal{K}$ data show an experimental scatter that is independent of the Reynolds number and of the fluid employed. It would be interesting to extend the range of $\mathcal{R}e$ to verify whether $\mathcal{K}$ reaches a constant value at larger $\mathcal{R}e$ and to quantify this value precisely. According to our measurements, $\lim_{\mathcal{R}e\to\infty} \mathcal{K}=0.9$ appears to be more realistic than the currently adopted $\mathcal{K}=1.1$. It is also important to investigate how $\mathcal{K}$ varies in the laminar-flow limit $\mathcal{R}e \to 0$.

Figure 7 shows a comparison between our $\mathcal{K}$ values as a function of $\mathcal{C}_f$ and the predicted $\mathcal{K}$ trend proposed by Crane [17] for turbulent flow conditions. Both Crane's formula [17] and our data predict that $\mathcal{K}$ increases monotonically with $\mathcal{C}_f$, but our data are lower than Crane's [17] in the whole $\mathcal{C}_f$ range. Furthermore, our study reveals that the increase of $\mathcal{K}$ with $\mathcal{C}_f$ is linear only for $0.02 < \mathcal{C}_f < 0.03$, while the dependence of $\mathcal{K}$ on $\mathcal{R}e$ is more significant for $\mathcal{C}_f > 0.03$. In the linear regime, the following relation between $\mathcal{K}$ and $\mathcal{C}_f$ is proposed,

$$\mathcal{K} = 26.92\mathcal{C}_f + 0.42, \quad 0.02 < \mathcal{C}_f < 0.03, \tag{5}$$

which fits the experimental data in this range of $\mathcal{C}_f$ within a ±2.5% average error. Crane [17] instead predicts a linear dependence for any value of $\mathcal{C}_f$, i.e. $\mathcal{K}=60\mathcal{C}_f$. It is worth noting that our linear correlation (5) does not cross the origin in the $(\mathcal{K}, \mathcal{C}_f)$ plane, while Crane's [17] does. If the straight line passed through the origin, the bulk velocity $\mathcal{U}_b^*$ could be simplified from the linear relationship upon re-writing the quantities in dimensional form. The elbow pressure drop could be computed by simply measuring the straight-pipe pressure drop and this would be very useful for engineering applications.

Figure 7 also shows that Kirchbach's [10] and Schubart's [11] data are also much lower than Crane's [17] predicted values, which is somewhat surprising because Crane's correlation [17] is based on Kirchbach's [10] and Schubart's [11] results.

For the whole range of $\mathcal{C}_f$ values, a new correlation relating $\mathcal{K}$ and $\mathcal{C}_f$ is proposed for flows across 90° sharp-angled elbows:

$$\mathcal{K} = 32980\,{\mathcal{C}_f}^{3.32} + 0.9, \quad 0.02 < \mathcal{C}_f < 0.05. \tag{6}$$

Correlation (6) fits the experimental data within a $\pm 1.9\%$ average error. If the well-known correlation for the turbulent friction coefficient given by Blasius, $\mathcal{C}_f = 0.3164\,\mathcal{R}e^{-0.25}$ [15], is substituted into our correlation (6), one obtains $\mathcal{K} = 722.8\mathcal{R}e^{-0.83} + 0.9$, which only differs from our correlation (4) by less than $\pm 2\%$, which is smaller than the experimental error of our $\mathcal{K}$ and $\mathcal{C}_f$ data.

As discussed in the Introduction, the equivalent length to diameter ratio,

$$\mathcal{L} = \frac{l^*_{eq}}{D^*} = \frac{l^*\Delta p^*_e}{D^*\Delta p^*}, \tag{7}$$

where the equivalent length l^*_{eq} is the length of the straight pipe that would generate the same pressure drop as the elbow at the same bulk Reynolds number, represents another way to express the pressure loss in elbows and pipe bends. In Eq. (7), l^* and Δp^* are defined as in Eq. (2). As shown in Fig. 8, $\mathcal{L}$ varies between 35 and 65. It decreases sharply up to $\mathcal{R}e$=7000, then increases slowly with $\mathcal{R}e$ and appears to approach the asymptotic value $\mathcal{L}$=45. Our data are in the middle of the experimental data for 90° round elbows by Wilson [19] (C=1) and Spedding [18] (C=0.65). The dashed line indicates the constant $\mathcal{L}$=60 suggested by Crane [17], which matches Spedding's data [18] at large Reynolds number. The dash-dotted line denotes the constant $\mathcal{L}$=43 proposed by Crawford [4], which shows the best agreement with our results. It is thus confirmed that $\mathcal{L}$ depends strongly on the elbow curvature ratio C and only mildly on $\mathcal{R}e$ for $\mathcal{R}e$>40000 [9, 8, 3, 4].

4 Summary

The pressure drop across 90° sharp-angled circular mitre elbows was investigated experimentally in the range of bulk Reynolds number 500<$\mathcal{R}e$<60000 by employing water and air as working fluids flowing through pipes with three different diameters. The straight-pipe friction factor shows excellent agreement with well-established correlations and reliable published data and it is proved that the pressure was axially symmetric at all the measurement locations. We have shown that the dependence of the pressure-loss coefficient of the mitre elbow on the bulk Reynolds number is rather pronounced, particularly for $\mathcal{R}e$<20000. We have also studied the relationship between this coefficient and the straight-pipe friction factor and obtained two new correlations for the pressure-loss coefficient which will be useful for the design of piping systems fitted with these sharp elbows. The pressure drop was also expressed in terms of the equivalent length to diameter ratio. We have shown that this ratio varies between 35 and 60 and we have presented its dependence on the Reynolds number.

5 Acknowledgements

The authors highly acknowledge the financial support by the Iraqi Ministry Of Higher Education and Scientific Research. The authors would like to thank Professor Kirill Horoshenkov, Professor Shuisheng He, Dr Giulio Dolcetti, Dr Elena Marensi, and Miss Eva Zincone for their useful comments.

References

[1] Dean, W., 1927. "Note on the motion of fluid in a curved pipe". *The London, Edinburgh, and Dublin Philosophical Magazine and J. Science,* **4**(20), pp. 208–223.

[2] Sugiyama, S., Hayashi, T., and Yamazaki, K., 1983. "Flow Characteristics in the Curved Rectangular Channels: Visualization of Secondary Flow". *Bulletin JSME,* **26**(216), pp. 964–969.

[3] Crawford, N., Cunningham, G., and Spedding, P., 2003. "Prediction of pressure drop for turbulent fluid flow in 90 bends". *Proc. Inst. Mech. Eng., Part E: J. Process Mech. Eng.,* **217**(3), pp. 153–155.

[4] Crawford, N., Cunningham, G., and Spence, S., 2007. "An experimental investigation into the pressure drop for turbulent flow in 90 elbow bends". *Proc. Ins. Mech. Part E: J. Process. Mech. Eng.,* **221**(2), pp. 77–88.

[5] Schmandt, B., and Herwig, H., 2012. "A standard method to determine loss coefficients of conduit components based on the second law of thermodynamics". In ASME Conference Proceedings, Paper No. ICNMM2012-73249.

[6] Schmandt, B., and Herwig, H., 2013. "Loss coefficients for periodically unsteady flows in conduit components: illustrated for laminar flow in a circular duct and a 90 degree bend". *ASME J. Fluids Eng.,* **135**(3), p. 031204.

[7] Schmandt, B., and Herwig, H., 2016. "Losses due to conduit components: an optimization strategy and its application". *ASME J. Fluids Eng.,* **138**(3), p. 031204.

[8] Beij, K., 1938. *Pressure Losses for Fluid Flow in 90° Pipe Bends*. National Bureau of Standards.

[9] Ito, H., 1960. "Pressure losses in smooth pipe bends". *ASME J. Fluids Eng.,* **82**(1), pp. 131–140.

[10] Kirchbach, H., 1935. "Loss of energy in miter bends". *Trans. Munich. Hydraulic Institute, American Soc. Mech. Eng.,* **3**.

[11] Schubart, W., 1935. "Energy loss in smooth-and rough-surfaced bends and curves in pipe lines". *Trans. Hydraul. Inst. Munich Tech. Univ,* **3**, pp. 81–99.

[12] Haidar, N., 1995. "Prediction of compressible flow pressure losses in 30–150 deg sharp-cornered bends". *ASME J. Fluids Eng.,* **117**(4), pp. 589–592.

[13] Moujaes, S., and Aekula, S., 2009. "Cfd predictions and experimental comparisons of pressure drop effects of turning vanes in 90 duct elbows". *J. Energy Eng.,* **135**(4), pp. 119–126.

[14] Munson, B., Young, D., and Okiishi, T., 2006. "Fundamentals of Fluid Mechanics, John Wiley & Sons". *John Wiley & Sons, Inc.*

[15] White, F., 2011. "Fluid mechanics. 7th". *Boston: McGraw-Hill Book Company*.

[16] Rennels, D., and Hudson, H., 2012. *Pipe Flow: A Practical and Comprehensive Guide*. John Wiley & Sons.

[17] Crane, 1988. *Flow of fluids through valves, fittings, and pipes*. Crane Co.

[18] Spedding, P., Benard, E., and McNally, G., 2004. "Fluid flow through 90 degree bends". *Developments in Chem. Eng. and Mineral Processing,* **12**(1-2), pp. 107–128.

[19] Wilson, R., McAdams, W., and Seltzer, M., 1922. "The flow of fluids through commercial pipe lines". *Ind. Eng. Chem.,* **14**(2), pp. 105–119.

[20] Perry, J., 1950. "Chemical Engineers' Handbook". *J. Chem. Educ.,* **27**(9), p. 533.

[21] Lemmon, E., Huber, M., and McLinden, M., 2010. NIST Standard Reference Database 23: Reference Fluid Thermodynamic and Transport Properties - REFPROP. 9.0.

[22] Taylor, J. R., 1997. *An Introduction to Error Analysis*. University Science Books.

[23] Churchill, S., 1977. "Friction-factor equation spans all fluid-flow regimes". *Chem. Eng.,* **84**(24), pp. 91–92.

[24] Haaland, S. E., 1983. "Simple and explicit formulas for the friction factor in turbulent pipe flow". *ASME J. Fluids Eng.,* **105**(1), pp. 89–90.

[25] McKeon, B., Swanson, C., Zagarola, M. V., Donnelly, R., and Smits, A., 2004. "Friction factors for smooth pipe flow". *J. Fluid Mech.,* **511**, pp. 41–44.

[26] den Toonder, J., and Nieuwstadt, F. M., 1997. "Reynolds number effects in a turbulent pipe flow for low to moderate Re". *Phys. Fluids,* **9**(11), pp. 3398–3409.
[27] Swanson, C., Julian, B., Ihas, G., and Donnelly, R., 2002. "Pipe flow measurements over a wide range of Reynolds numbers using liquid helium and various gases". *J. Fluid Mech.,* **461**, pp. 51–60.
[28] Wu, X., and Moin, P., 2008. "A direct numerical simulation study on the mean velocity characteristics in turbulent pipe flow". *J. Fluid Mech.,* **608**, pp. 81–112.

A Computation of the pressure-loss coefficient and scaled equivalent length

Figure 9 shows the scaled pressure drop along the test sections and across the mitre elbows for water and air flows. The trends show the independence of the results on the working fluid and clearly show the local drop due to the elbow. This effect is negligible upstream and downstream of streamwise distances equal to $32.5D^*$ from the elbow (measurement locations C and F, respectively), i.e. where the pressure gradient is solely due to the distributed straight-pipe frictional effects.

As displayed in Fig. 9, the pressure-drop coefficient $\mathcal{K}$ was computed as the difference between the intercepts on the vertical axis of the two best-fit straight lines defining the straight-pipe pressure gradients upstream and downstream of locations C and F (dashed red lines). The scaled equivalent length $\mathcal{L}$ was obtained by subtracting the intercepts of the two best-fit straight lines on the horizontal axis.

B Measurement of peripheral pressure

Figure 10 shows scaled air pressure measurements at different angles (0°, 90° and 270°) around the periphery of the 16-mm-diameter pipe at four different stations upstream and downstream of the elbow and at four Reynolds numbers. The experimental data show that the peripheral pressure upstream and downstream of the elbow is axially symmetric at all the tested locations. As shown in Fig. 3, the closest locations D and E are at a distance of $7D^*$ upstream and downstream of the elbow, respectively, which agrees with the result by Ito for 90° round elbows [9].

List of figures

List of tables

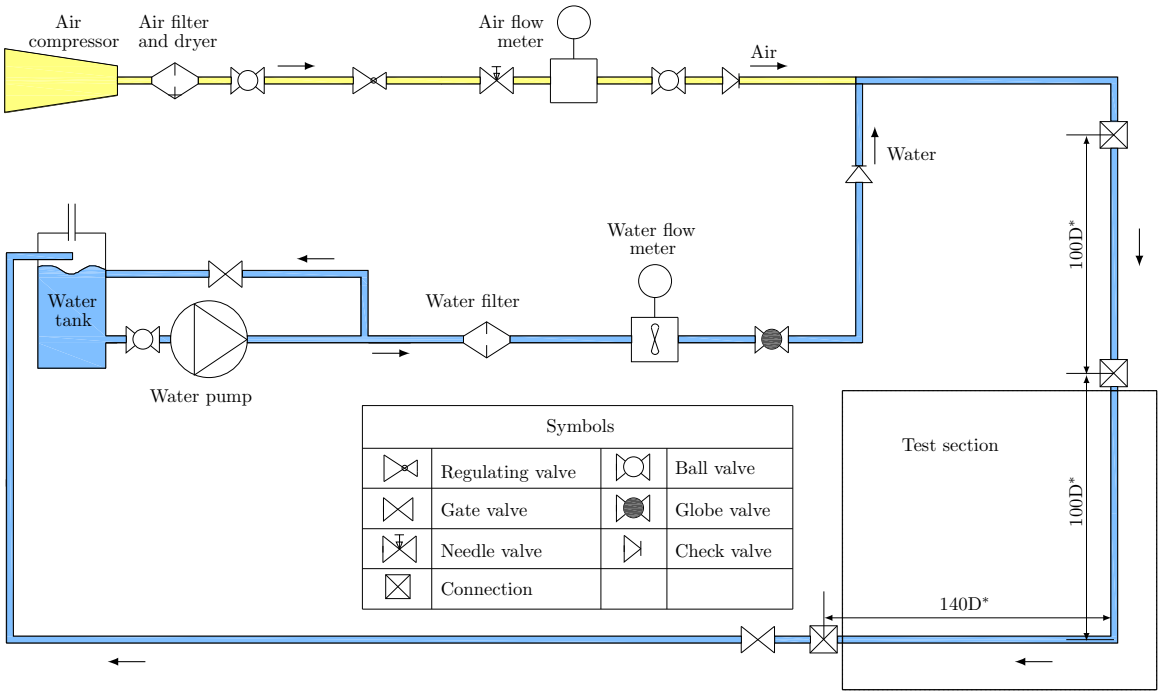

Fig. 1. Schematic diagram of the experimental facility.

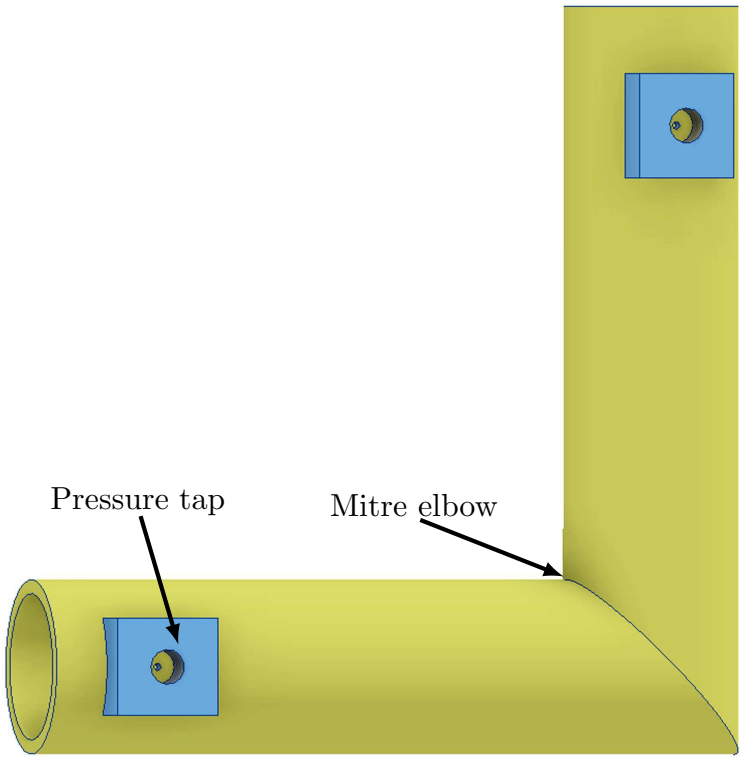

Fig. 2. Schematic diagram of the 90° sharp-angled elbow and pressure tap.

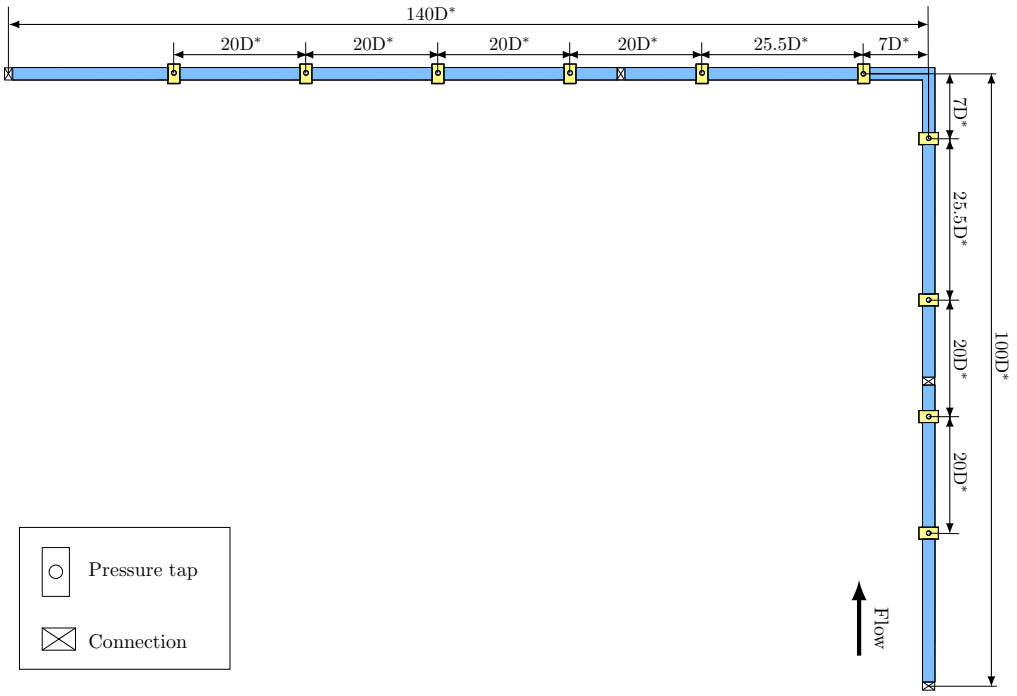

Fig. 3. Schematic diagram of the test sections.

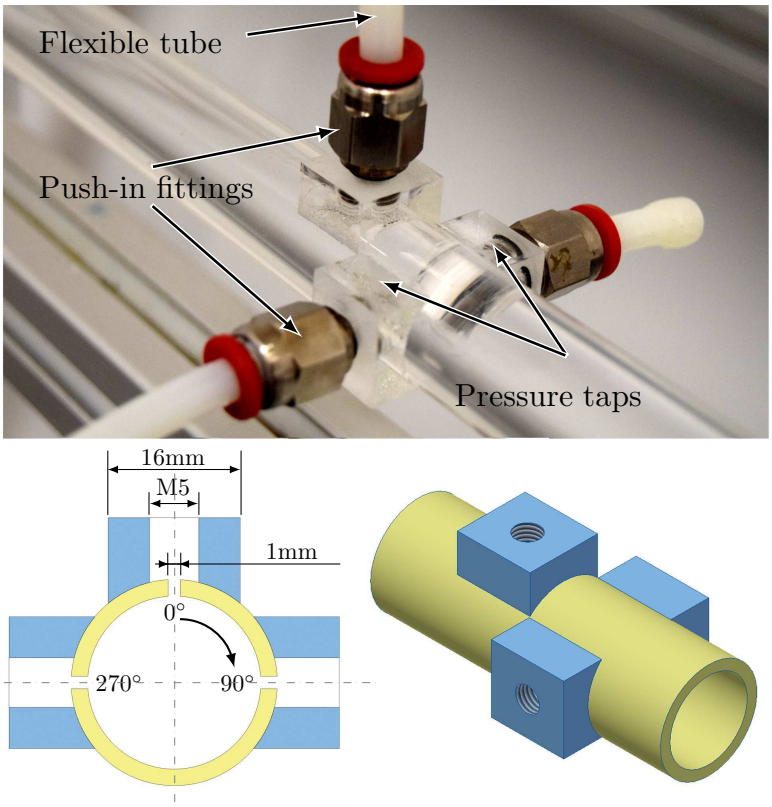

Fig. 4. Picture and schematic diagram of the pressure taps.

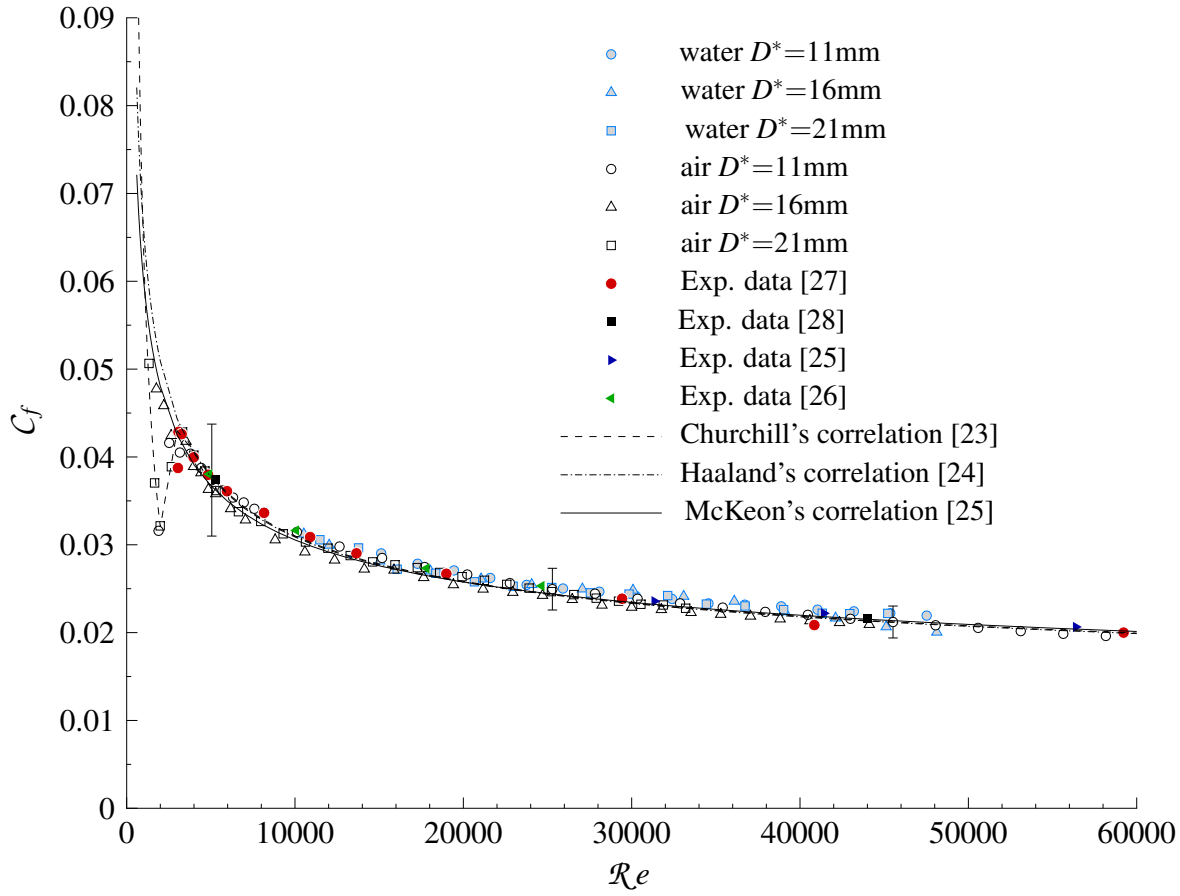

Fig. 5. Friction factor C_f as a function of the Reynolds number $\mathcal{R}e$ for flow through straight pipes.

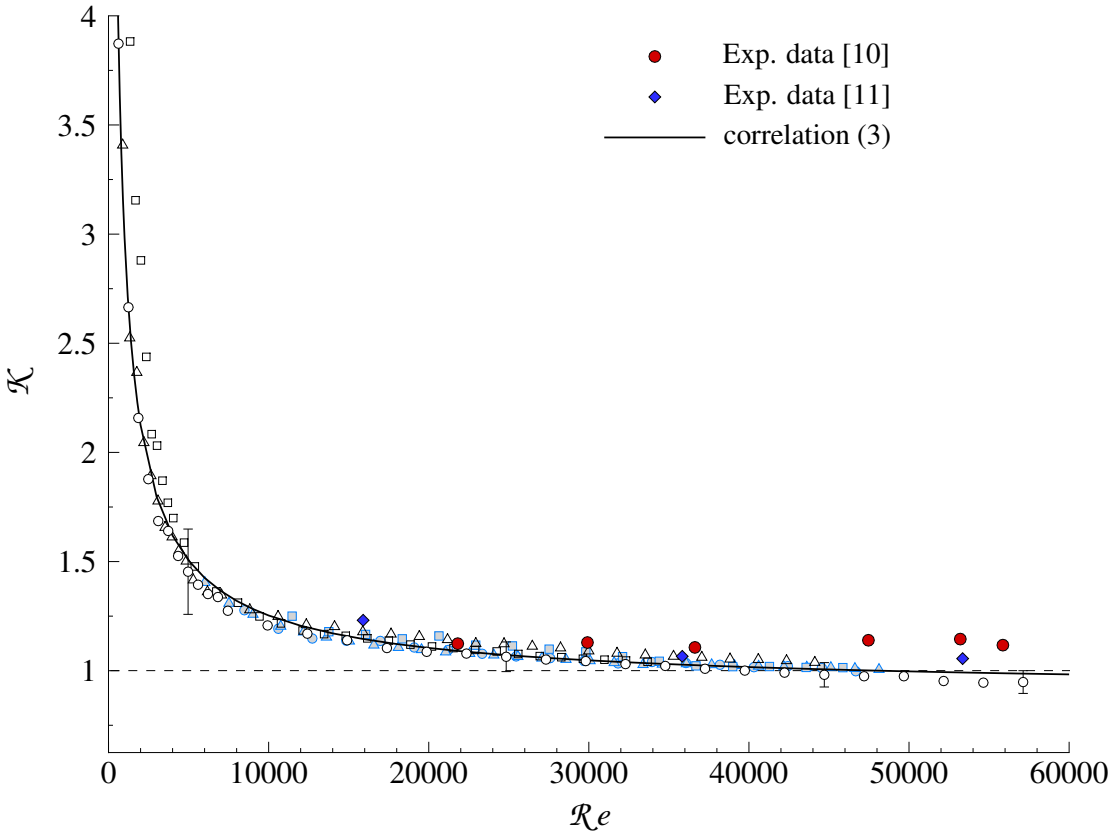

Fig. 6. Pressure-loss coefficient $\mathcal{K}$ for 90° sharp-angled elbows as a function of the Reynolds number $\mathcal{R}e$. The symbols are given in Fig. 5.

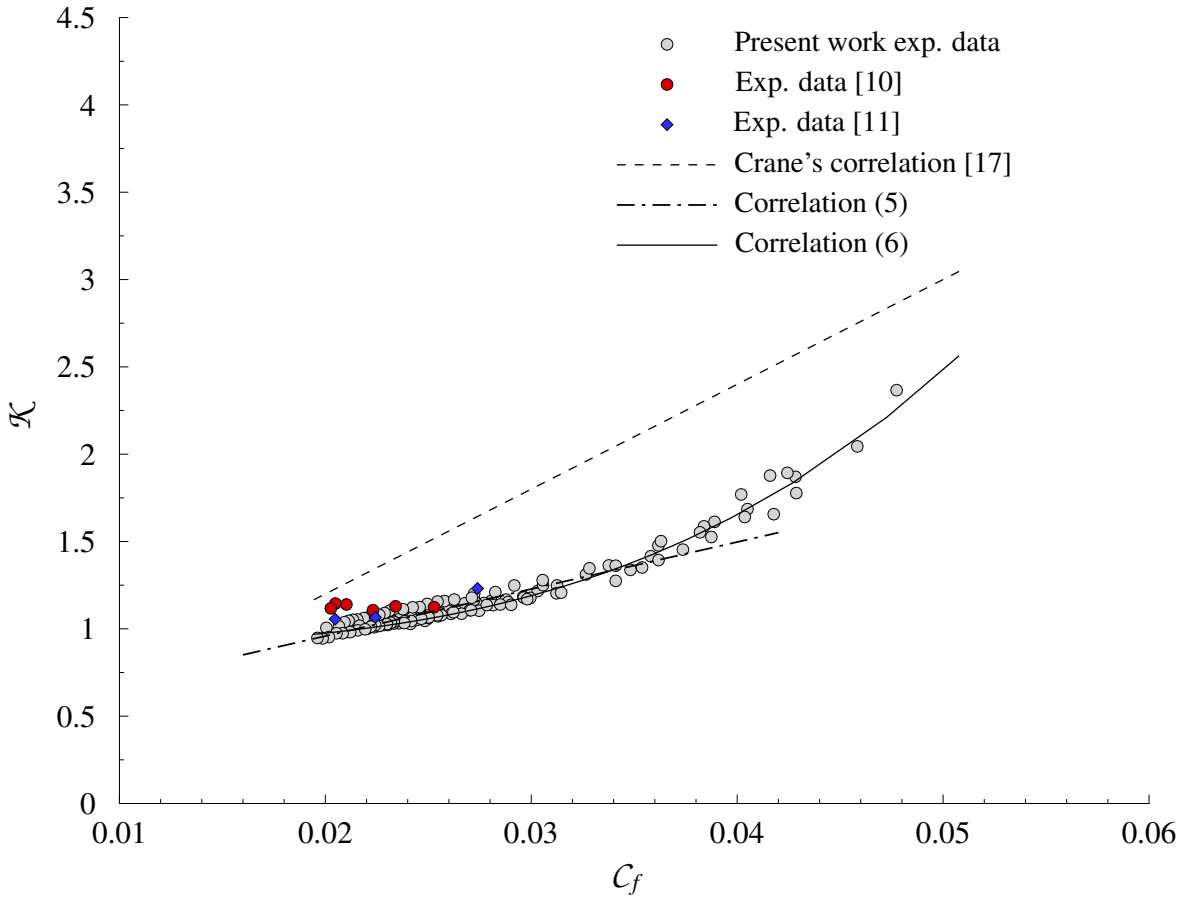

Fig. 7. Pressure-loss coefficient $\mathcal{K}$ for sharp-angled elbows as a function of C_f.

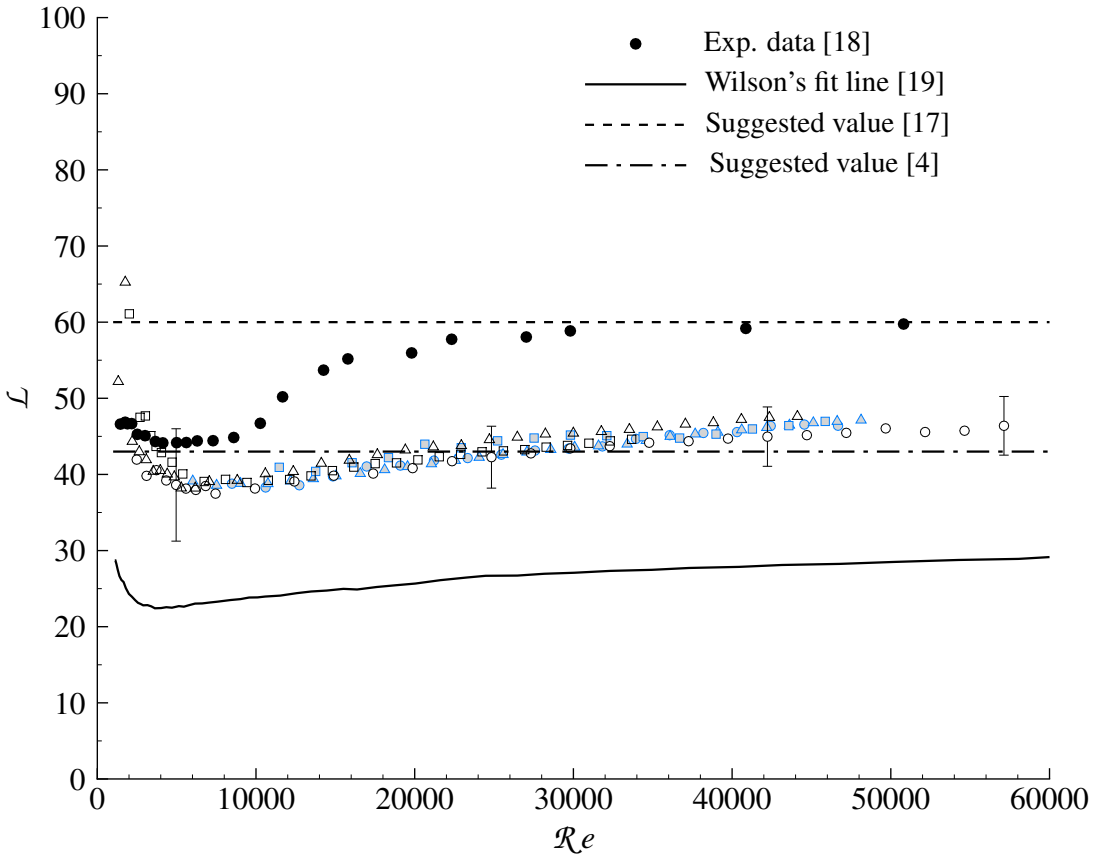

Fig. 8. Equivalent length to diameter ratio $\mathcal{L}$ for sharp-angled elbow as a function of $\mathcal{R}e$. The symbols are given in Fig. 5.

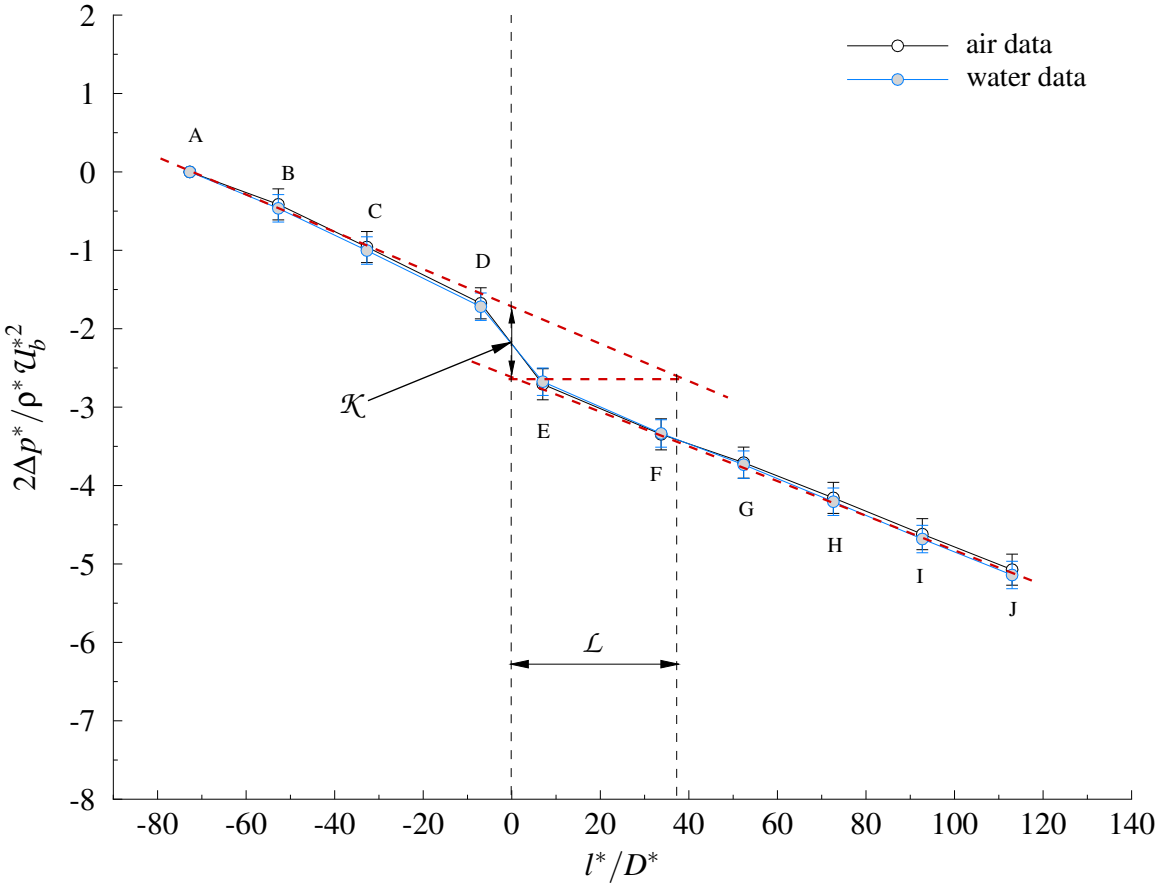

Fig. 9. Pressure drop relative to the measurement location A along the 11-mm-diameter test section at $\mathcal{R}e = 17000$ for air and water flows. The pressure-loss coefficient $\mathcal{K}$ and the scaled equivalent length $\mathcal{L}$ are indicated.

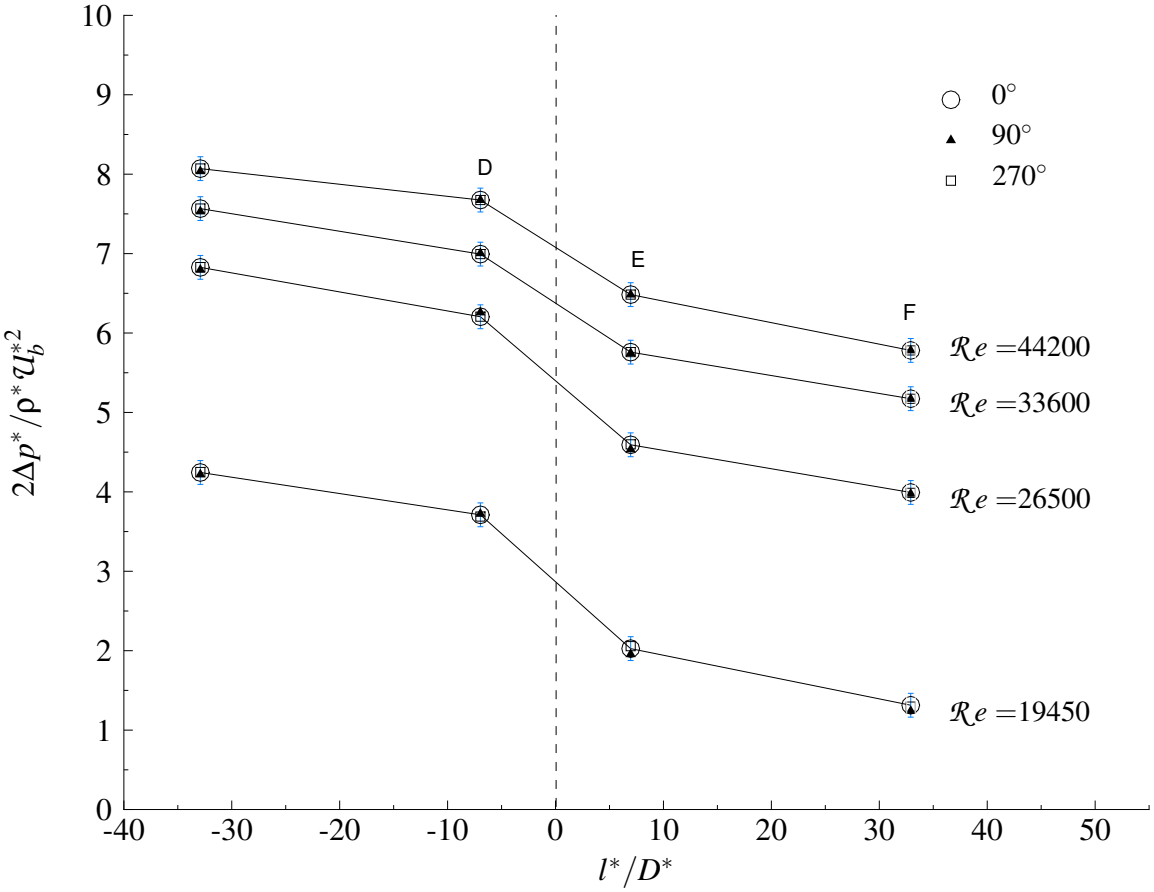

Fig. 10. Air-flow pressure drop at different angles around the pipe periphery at stations C, D, E and F of the 16-mm-diameter test section at different Reynolds numbers.

Table 1. Water and air flow rates.

D^* (mm)	Water flow (l/min)	Air flow (standard l/min)
11	4-22	5-460
16	4-32	10-500
21	4-40	15-500